Perturbation Schemes for Passivity Enforcement of Delay-Based Transmission Line Macromodels

Alessandro Chinea and Stefano Grivet-Talocia, *Senior Member, IEEE*

***Abstract*—This paper introduces two different algorithms for passivity enforcement of transmission-line macromodels based on the generalized method of characteristics (MoC). The first scheme corrects passivity violations via perturbation of purely imaginary solutions of a nonlinear Hamiltonian eigenvalue problem. The second scheme is based on a linearly constrained quadratic optimization formulated at carefully selected frequency samples. Both schemes can be viewed as extensions to the case of MoC-based macromodels of existing techniques that were only available for lumped macromodels. The resulting passive delay-based macromodels can be safely employed in system-level signal integrity simulations, due to their inability to produce any spurious energy gain. Several numerical examples illustrate the behavior of both schemes on transmission line structures of practical interest, highlighting their main differences and the open problems deserving further research work.**

***Index Terms*— Hamiltonian matrices, method of characteristics, passivity, perturbation, transmission lines.**

I. Introduction

LINEAR macromodeling has become a standard practice for the analysis and design of electrical interconnects. Macromodels provide simplified approximations of the terminal port behavior of possibly complex interconnect structures and allow very fast transient simulations using standard circuit solvers. Therefore, a lot of research activities have been carried out during the recent years, trying to define numerically robust methodologies for the identification of macromodels known either from electromagnetic simulation or direct measurement [1]–[12].

In this work, we concentrate on the problem of transmission-line macromodeling. Transmission lines are inherently of distributed nature, with possibly large propagation delays. When conductor and dielectric losses are included in the model, difficulties arise in the conversion of frequency-domain telegraphers equations to a circuit stamp that can be efficiently used in a standard transient solver. Many approaches have been presented for this task [13]–[24], mainly differing on how the propagation delay is handled. Some methods approximate the delay term with rational functions, leading to lumped macromodels, see e.g., [14]–[17]. Some other techniques try to extract the delay [18]–[24], leading to much more efficient models for long lines. In particular, macromodels based on the generalized method of characteristics (MoC) are widely recognized as the most efficient [19]–[24] for structures with significant propagation delay. Therefore, we will concentrate on this macromodel class.

Interconnect macromodels must be passive. If this property is not fulfilled, instabilities may arise during time-domain simulation, due to an unphysical energy gain produced by the model [32], [35]. The enforcement of passivity is a quite challenging problem, which still presents several open issues. For instance, several algorithms are available for the generation of guaranteed passive lumped macromodels [25]–[41]. However, for delay-based transmission line macromodels with MoC structure, there is currently no general method allowing to enforce passivity. In [44], [45], [46], a fundamental result has been achieved, by providing a theoretical formalization of the MoC structure by casting the model equations in a form that allows a purely algebraic passivity check. These results have been exploited in [47], [48] to derive a preliminary scheme for a posteriori passivity correction. An alternative method, applicable to scalar lines only, is available in [49].

In this work, we extend the results of [47], [48] by providing two alternative perturbation schemes for passivity enforcement of MoC-based transmission line macromodels. The results in this paper strongly depend on the background material in [46], which is shortly recalled in Sections II and III. The two passivity enforcement schemes are presented in Section IV and applied to practical application examples in Section V. Section VI discusses the main results and draws some conclusions.

II. Preliminaries

We consider a lossy multiconductor transmission line of length $\mathcal{L}$ described, in the Laplace domain, by the telegraphers equations

$$\begin{aligned} -\frac{\mathrm{d}}{\mathrm{d}z}\boldsymbol{V}(z,s) &= (\boldsymbol{R}(s)+s\boldsymbol{L}(s))\boldsymbol{I}(z,s) \\ -\frac{\mathrm{d}}{\mathrm{d}z}\boldsymbol{I}(z,s) &= (\boldsymbol{G}(s)+s\boldsymbol{C}(s))\boldsymbol{V}(z,s) \end{aligned} \tag{1}$$

where z is the longitudinal coordinate, $\boldsymbol{R}(s), \boldsymbol{L}(s), \boldsymbol{G}(s)$, and $\boldsymbol{C}(s)$ denote the $m \times m$ frequency dependent per-unit-length (f-PUL) resistance, inductance, conductance and capacitance matrices, respectively. Following the method of characteristic (MoC) approach, the solution is written as [24]

$$\begin{aligned} \boldsymbol{I}_1(s) &= \boldsymbol{Y}_c(s)\boldsymbol{V}_1(s) \\ &\quad - \boldsymbol{Q}(s)[\boldsymbol{Y}_c(s)\boldsymbol{V}_2(s)+\boldsymbol{I}_2(s)] \\ \boldsymbol{I}_2(s) &= \boldsymbol{Y}_c(s)\boldsymbol{V}_2(s) \\ &\quad - \boldsymbol{Q}(s)[\boldsymbol{Y}_c(s)\boldsymbol{V}_1(s)+\boldsymbol{I}_1(s)] \end{aligned} \tag{2}$$

Manuscript received July 31, 2007; revised December 13, 2007. First published May 31, 2008; last published August 6, 2008 (projected). This work was recommended for publication by Associate Editor A. Maffucci upon evaluation of the reviewers comments.

The authors are with the Department of Electronics, Politecnico di Torino, 10129 Torino, Italy (e-mail: alessandro.chinea@polito.it; stefano.grivet@polito.it).

Digital Object Identifier 10.1109/TADVP.2008.920642

where $\boldsymbol{V}_{1,2}(s)$ and $\boldsymbol{I}_{1,2}(s)$ represent the terminal voltages and currents of the line and where $\boldsymbol{Q}(s) = \exp\{-\boldsymbol{\Gamma}(s)\mathcal{L}\}, \boldsymbol{\Gamma}^2(s) = \boldsymbol{Y}(s)\boldsymbol{Z}(s)$, and $\boldsymbol{Y}_c(s) = \boldsymbol{\Gamma}^{-1}(s)\boldsymbol{Y}(s)$ are the propagation operator, propagation constant, and characteristic admittance matrices, respectively. A SPICE-compatible stamp is derived from (2) by extracting the asymptotic modal delays $\boldsymbol{T} = \mathrm{diag}\{T_k\}$ from the propagation operator $\boldsymbol{Q}(s)$

$$\boldsymbol{P}(s) = e^{-s\boldsymbol{T}}\boldsymbol{M}^{-1}\boldsymbol{Q}(s)\boldsymbol{M} \tag{3}$$

using the asymptotic modal decomposition matrix $\boldsymbol{M}$, and by approximating the remaining matrix operators $\boldsymbol{Y}_c(s), \boldsymbol{P}(s)$ with low-order rational functions $\tilde{\boldsymbol{Y}}_c(s), \tilde{\boldsymbol{P}}(s)$, respectively. The well-known vector fitting algorithm [1] can be used for this task, leading to the state-space realizations

$$\begin{aligned}\tilde{\boldsymbol{Y}}_c(s) &= \bar{\boldsymbol{C}}(s\boldsymbol{U} - \bar{\boldsymbol{A}})^{-1}\bar{\boldsymbol{B}} + \bar{\boldsymbol{D}}\\ \tilde{\boldsymbol{P}}(s) &= \hat{\boldsymbol{C}}(s\boldsymbol{U} - \hat{\boldsymbol{A}})^{-1}\hat{\boldsymbol{B}} + \hat{\boldsymbol{D}}\end{aligned} \tag{4}$$

where $\boldsymbol{U}$ denotes the identity matrix. The MoC macromodel can be characterized using the short-circuit admittance matrix $\boldsymbol{Y}(s)$, which can be obtained as in [44] from (2)—(4)

$$\boldsymbol{Y}(s) = \begin{bmatrix} \boldsymbol{W}_0^{-1}(s)\boldsymbol{W}_1(s)\tilde{\boldsymbol{Y}}_c(s) & \boldsymbol{W}_0^{-1}(s)\boldsymbol{W}_2(s)\tilde{\boldsymbol{Y}}_c(s) \\ \boldsymbol{W}_0^{-1}(s)\boldsymbol{W}_2(s)\tilde{\boldsymbol{Y}}_c(s) & \boldsymbol{W}_0^{-1}(s)\boldsymbol{W}_1(s)\tilde{\boldsymbol{Y}}_c(s)\end{bmatrix} \tag{5}$$

where

$$\begin{aligned}\boldsymbol{W}_0 &= \boldsymbol{U} - \boldsymbol{M}\mathrm{e}^{-s\boldsymbol{T}}\tilde{\boldsymbol{P}}(s)\mathrm{e}^{-s\boldsymbol{T}}\tilde{\boldsymbol{P}}(s)\boldsymbol{M}^{-1}\\ \boldsymbol{W}_1 &= \boldsymbol{U} + \boldsymbol{M}\mathrm{e}^{-s\boldsymbol{T}}\tilde{\boldsymbol{P}}(s)\mathrm{e}^{-s\boldsymbol{T}}\tilde{\boldsymbol{P}}(s)\boldsymbol{M}^{-1}\\ \boldsymbol{W}_2 &= -2\boldsymbol{M}\mathrm{e}^{-s\boldsymbol{T}}\tilde{\boldsymbol{P}}(s)\boldsymbol{M}^{-1}.\end{aligned} \tag{6}$$

III. Passivity Characterization

It is well known that a model is passive if and only if its admittance matrix $\boldsymbol{Y}(s)$ is positive real. If $\tilde{\boldsymbol{Y}}_c(s), \tilde{\boldsymbol{P}}(s)$, and $\boldsymbol{Y}(s)$ are asymptotically stable (do not have poles in the closed right-half plane of the s-domain) with $\tilde{\boldsymbol{P}}(s) \to 0$ for $s \to \infty$, the positive realness of $\boldsymbol{Y}(s)$ is equivalent to the condition

$$\boldsymbol{G}(s) = \boldsymbol{Y}(s) + \boldsymbol{Y}^T(-s) \geq 0, \quad \forall s = j\omega. \tag{7}$$

The latter condition can be further simplified [46], by requiring that the two subsystems $\boldsymbol{G}_{1,2}(s)$ defined as

$$\boldsymbol{G}_{1,2} = \boldsymbol{\Upsilon}_{1,2}(s) + \boldsymbol{\Upsilon}_{1,2}^T(-s) \geq 0, \quad \forall s = j\omega \tag{8}$$

are nonnegative definite, where

$$\begin{aligned}\boldsymbol{\Upsilon}_{1,2}(s) &= \boldsymbol{W}_{\pm}^{-1}(s)\boldsymbol{W}_{\mp}(s)\tilde{\boldsymbol{Y}}_c(s)\\ \boldsymbol{W}_{\pm}(s) &= \boldsymbol{U} \pm \boldsymbol{M}e^{-s\boldsymbol{T}}\tilde{\boldsymbol{P}}(s)\boldsymbol{M}^{-1}.\end{aligned} \tag{9}$$

Following the procedure in [46], we can derive a time-domain representation of these subsystems via inverse Laplace transform combined by simple algebraic manipulations. First, we define

$$\Sigma_{\pm} : \begin{cases} \dot{\boldsymbol{x}}(t) = \boldsymbol{A}\boldsymbol{x}(t) + \boldsymbol{B}\boldsymbol{u}(t) \\ \boldsymbol{y}(t) = \pm\sum_{n=1}^{m}\boldsymbol{C}^n\boldsymbol{x}(t - T_n) + \boldsymbol{D}\boldsymbol{u}(t)\end{cases} \tag{10}$$

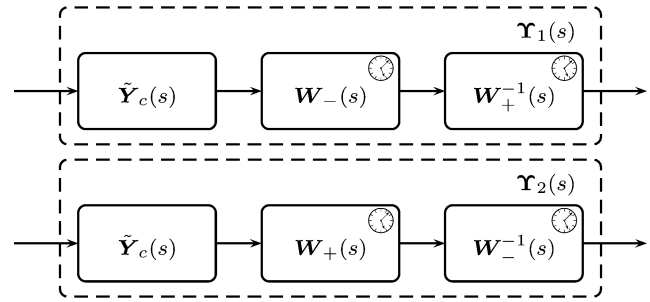

Fig. 1. Graphical illustration of the internal structure of the two subsystems $\boldsymbol{\Upsilon}_{1,2}(s)$. See also text. The small clock icon denotes a dynamical system with time delays.

as the delayed state-space realization of $\boldsymbol{W}_{\pm}(s)$. Then, a delayed state-space realization of $\boldsymbol{\Upsilon}_{1,2}(s)$ is obtained by cascading the three partial realizations of $\tilde{\boldsymbol{Y}}_c(s)$ and $\boldsymbol{W}_{\pm}(s)$ according to (9), as illustrated in Fig. 1. Detailed expressions of all matrices are reported in [46] and are not repeated here.

Also in [46], it is proved that the nonnegative definiteness of $\boldsymbol{\Upsilon}_{1,2}(s)$ is equivalent to requiring that there are no simple pure imaginary eigenvalues satisfying the two following frequency-dependent eigenvalue problems (FD-EP):

$$s\boldsymbol{\xi} = \boldsymbol{H}_{1,2}(s)\boldsymbol{\xi} \tag{11}$$

where

$$\boldsymbol{H}_{1,2}(s) = \boldsymbol{\mathcal{V}} \pm \sum_{n=1}^{m}\left(\boldsymbol{\mathcal{W}}_n^- e^{-sT_n} + \boldsymbol{\mathcal{W}}_n^+ e^{sT_n}\right) + \sum_{n=1}^{m}\sum_{l=1}^{m}\boldsymbol{\mathcal{W}}_{n,l}e^{s(T_n - T_l)}. \tag{12}$$

The constant matrices $\boldsymbol{\mathcal{V}}, \boldsymbol{\mathcal{W}}^+, \boldsymbol{\mathcal{W}}^-$ and $\boldsymbol{\mathcal{W}}_{n,l}$ are given in terms of the state-space realizations in (4) and (10). Their detailed expressions are as follows:

$$\begin{aligned}\boldsymbol{\mathcal{V}} &= \begin{bmatrix}\boldsymbol{\mathcal{V}}_{11} & \boldsymbol{\mathcal{V}}_{12}\\ \boldsymbol{\mathcal{V}}_{21} & -\boldsymbol{\mathcal{V}}_{11}^T\end{bmatrix}\\ \boldsymbol{\mathcal{W}}_n^- &= \begin{bmatrix}\boldsymbol{\mathcal{W}}_{11,n}^- & \boldsymbol{0}\\ \boldsymbol{\mathcal{W}}_{21,n}^- & \boldsymbol{0}\end{bmatrix}\\ \boldsymbol{\mathcal{W}}_n^+ &= \begin{bmatrix}\boldsymbol{0} & \boldsymbol{0}\\ (\boldsymbol{\mathcal{W}}_{21,n}^-)^T & -(\boldsymbol{\mathcal{W}}_{11,n}^-)^T\end{bmatrix}\\ \boldsymbol{\mathcal{W}}_{n,l} &= \begin{bmatrix}\boldsymbol{0} & \boldsymbol{0}\\ \boldsymbol{\mathcal{W}}_{21,n,l} & \boldsymbol{0}\end{bmatrix}\end{aligned} \tag{13}$$

$$\begin{aligned}\boldsymbol{\mathcal{V}}_{11} &= \begin{bmatrix}\boldsymbol{A} & \boldsymbol{0} & \hat{\boldsymbol{B}}_1\boldsymbol{\mathcal{R}}\boldsymbol{D}\bar{\boldsymbol{C}}\\ \boldsymbol{0} & \boldsymbol{A} & \hat{\boldsymbol{B}}_2\boldsymbol{\mathcal{R}}\boldsymbol{D}\bar{\boldsymbol{C}} + \boldsymbol{B}\bar{\boldsymbol{C}}\\ \boldsymbol{0} & \boldsymbol{0} & \bar{\boldsymbol{A}} + \hat{\boldsymbol{B}}_3\boldsymbol{\mathcal{R}}\boldsymbol{D}\bar{\boldsymbol{C}}\end{bmatrix}\\ \boldsymbol{\mathcal{V}}_{12} &= \begin{bmatrix}\hat{\boldsymbol{B}}_1\boldsymbol{\mathcal{R}}\hat{\boldsymbol{B}}_1^T & \hat{\boldsymbol{B}}_{12} & \hat{\boldsymbol{B}}_{13}\\ \hat{\boldsymbol{B}}_{12}^T & \hat{\boldsymbol{B}}_2\boldsymbol{\mathcal{R}}\hat{\boldsymbol{B}}_2^T & \hat{\boldsymbol{B}}_2\boldsymbol{\mathcal{R}}\hat{\boldsymbol{B}}_3^T\\ \hat{\boldsymbol{B}}_{13}^T & \hat{\boldsymbol{B}}_3\boldsymbol{\mathcal{R}}\hat{\boldsymbol{B}}_2^T & \hat{\boldsymbol{B}}_3\boldsymbol{\mathcal{R}}\hat{\boldsymbol{B}}_3^T\end{bmatrix}\\ \boldsymbol{\mathcal{V}}_{21} &= \begin{bmatrix}\boldsymbol{0} & \boldsymbol{0} & \boldsymbol{0}\\ \boldsymbol{0} & \boldsymbol{0} & \boldsymbol{0}\\ \boldsymbol{0} & \boldsymbol{0} & -\bar{\boldsymbol{C}}^T\boldsymbol{D}^T\boldsymbol{\mathcal{R}}\boldsymbol{D}\bar{\boldsymbol{C}}\end{bmatrix}\end{aligned} \tag{14}$$

$$\mathcal{W}_{11,n}^{-} = \begin{bmatrix} \hat{B}_1 \mathcal{R} C^n & -\hat{B}_1 \mathcal{R} C^n & \mathbf{0} \\ \hat{B}_2 \mathcal{R} C^n & -\hat{B}_2 \mathcal{R} C^n & \mathbf{0} \\ \hat{B}_3 \mathcal{R} C^n & -\hat{B}_3 \mathcal{R} C^n & \mathbf{0} \end{bmatrix}$$

$$\mathcal{W}_{21,n}^{-} = \begin{bmatrix} \mathbf{0} & \mathbf{0} & \mathbf{0} \\ \mathbf{0} & \mathbf{0} & \mathbf{0} \\ -\bar{C}^T D^T \mathcal{R} C^n & \bar{C}^T D^T \mathcal{R} C^n & \mathbf{0} \end{bmatrix} \quad (15)$$

$$\mathcal{W}_{21,n,l} = \begin{bmatrix} -(C^n)^T \mathcal{R} C^l & (C^n)^T \mathcal{R} C^l & \mathbf{0} \\ (C^n)^T \mathcal{R} C^l & -(C^n)^T \mathcal{R} C^l & \mathbf{0} \\ \mathbf{0} & \mathbf{0} & \mathbf{0} \end{bmatrix} \quad (16)$$

$$\begin{aligned} \mathcal{R} &= -(D\bar{D}D^T + D\bar{D}^T D^T)^{-1} \\ \hat{B}_1 &= B\bar{D}^T D^T \\ \hat{B}_2 &= B\bar{D}D^T \\ \hat{B}_3 &= \bar{B}D^T \\ \hat{B}_{12} &= \hat{B}_1 \mathcal{R} \hat{B}_2^T + B\bar{D}^T B^T \\ \hat{B}_{13} &= \hat{B}_1 \mathcal{R} \hat{B}_3^T + B\bar{B}^T. \end{aligned} \quad (17)$$

A tedious but simple check shows that $\boldsymbol{H}_{1,2}(s)$ are Hamiltonian matrices for $s = j\omega$, i.e.,

$$\boldsymbol{J}^{-1} \boldsymbol{H}_{1,2}(j\omega) \boldsymbol{J} = -\boldsymbol{H}_{1,2}^H(j\omega) \quad (18)$$

where

$$\boldsymbol{J} = \begin{bmatrix} \mathbf{0} & U \\ -U & \mathbf{0} \end{bmatrix}. \quad (19)$$

The Hamiltonian structure will be useful in the following.

The result in (11) is very important under a theoretical standpoint, since, in principle, it allows checking model passivity via algebraic eigenvalue conditions (11), thus avoiding any direct frequency sampling process applied to (7). On the other hand, the solution of (11) is a quite challenging numerical task, since standard algorithms for nonlinear eigenvalue problems may easily become ill-conditioned even for a moderate matrix size. Due to these difficulties, the approach in [46] performs an initial frequency sampling to find the regions where imaginary eigenvalues are potentially present. Then, using a suitable Chebychev polynomial approximation, the FDEP in (11) is transformed in a local polynomial eigenvalue problem, which is more tractable. Nonetheless, we have experienced numerical difficulties in the application of this approach when more eigenvalues are clustered in small frequency bands. This situation typically occurs when the number of line conductors grows, as will be shown in Section V.

In order to overcome these problems, we step back and resort to a more conservative adaptive frequency sampling process, similar to [36] and [37]. The generalized Hamiltonian formulation (11) will however play a key role in the formulation of the passivity enforcement scheme based on the eigenvalue perturbation, see Section IV-A. Passivity check is here based on a direct verification of the conditions (7), by explicitly computing the eigenvalues of $\boldsymbol{G}_{1,2}$ at carefully selected frequency points. The guidelines for the definition of the highest frequency sample and the sampling interval are given below.

- An upper frequency limiting the region where imaginary solutions to (11) can be located can be derived by applying the triangle inequality to matrix $\boldsymbol{H}_{1,2}(j\omega)$. Using (12) and omitting subscripts, we can write

$$\begin{aligned} \|\boldsymbol{H}(j\omega)\| &\le \|\mathcal{V}\| + \sum_{n=1}^{m} \|\mathcal{W}_n^{-} e^{-j\omega T_n}\| \\ &\quad + \sum_{n=1}^{m} \|\mathcal{W}_n^{+} e^{j\omega T_n}\| \\ &\quad + \sum_{n=1}^{m} \sum_{l=1}^{m} \|\mathcal{W}_{n,l} e^{j\omega(T_n - T_l)}\| \\ &= \|\mathcal{V}\| + \sum_{n=1}^{m} \|\mathcal{W}_n^{-}\| + \sum_{n=1}^{m} \|\mathcal{W}_n^{+}\| \\ &\quad + \sum_{n=1}^{m} \sum_{l=1}^{m} \|\mathcal{W}_{n,l}\| \end{aligned} \quad (20)$$

  where the adopted norm $\|\cdot\|$ denotes the maximum singular value of its matrix argument. We also have [54]

$$\rho(\boldsymbol{H}(j\omega)) \le \|\boldsymbol{H}(j\omega)\| \quad (21)$$

  where $\rho(\cdot)$ is the spectral radius defined as

$$\rho(\boldsymbol{H}(j\omega)) = \max_i \{|\lambda_i| : \lambda_i \in \lambda\{\boldsymbol{H}(j\omega)\}\} \quad (22)$$

  with $\lambda\{\boldsymbol{H}(j\omega)\}$ denoting the set of all eigenvalues. Combining (20) and (21), we obtain an explicit upper bound for all eigenvalues of $\boldsymbol{H}(j\omega)$, independent of $j\omega$, and therefore also valid for all the solutions of the FD-EPs (11). We use this bound to limit the frequency interval to be searched.
- The sampling interval is defined by noticing that the elements of $\boldsymbol{\Upsilon}_{1,2}$ in (9) are linear combinations of delay elements, the largest delay being $2\max_k T_k$. It is sufficient to sample with at least $N = 20 - 30$ points the corresponding minimum period, resulting in a frequency resolution

$$\delta\omega \le \frac{\pi}{N \max_k \{T_k\}}. \quad (23)$$

  Additional frequency samples are located near each pole of $\tilde{\boldsymbol{Y}}_c(s)$ and $\tilde{\boldsymbol{P}}(s)$, in order to capture possible fast eigenvalue variations induced by the macromodel poles.
- The above rules give an initial set of frequency samples. Then, an iterative refinement process is started to find the zero crossings of each eigenvalue up to arbitrary precision. This is achieved by a combination of eigenvalue tracking and iterative bisection, as detailed in [37].

The outcome of the proposed passivity check algorithm is depicted in Fig. 2 for a 5-conductor coupled stripline structure, whose detailed analysis is postponed to Section V. The figure shows the five eigenvalues of $\boldsymbol{G}_1$ (the corresponding ones for $\boldsymbol{G}_2$ result positive and are not shown) as functions of frequency, plotted using all frequency samples selected by the above procedure. Only a zoom on the frequency interval where passivity violations are found (highlighted by the shaded areas) is depicted. The dots denote the crossings with the zero baseline and correspond to the solutions of the FDEP (11).

For this case, the initial number of frequency points was set to 105, and we used a very stringent relative accuracy threshold $\epsilon = 1 \times 10^{-12}$ to stop the iterative refinement process. The final number of frequency samples was 1720. The computing time required to find these results is 6.5 s on a notebook (1.66 GHz

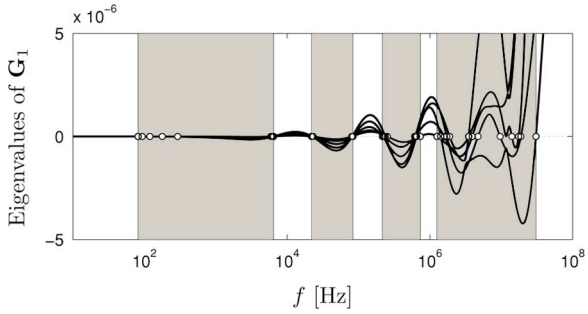

Fig. 2. Results of the passivity check for a 5-conductor coupled stripline. Frequency-dependent eigenvalues of G_1 are plotted (solid lines) with the corresponding zero-crossings (dots), which are the solutions of the FDEP in (11). Passivity violation intervals are highlighted.

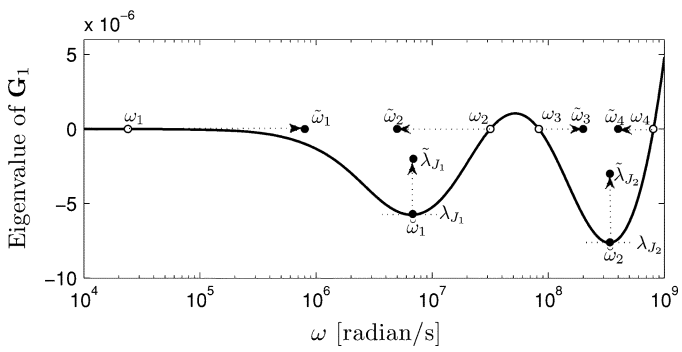

Fig. 3. Graphical illustration of horizontal and vertical displacement schemes for MoC passivity enforcement (see text).

CPU). We remark that the direct solution of the FDEP problem (11) could not find all eigenvalues to a precision sufficient to ascertain if they were purely imaginary, and it took longer (75 s on the same computer).

IV. Passivity Enforcement

This paper presents two alternative algorithms for MoC passivity enforcement. Both schemes share the common objective of removing the passivity violation intervals, but use different perturbation approaches to meet this goal. We introduce them qualitatively with the support of Fig. 3. We label the first scheme, detailed in Section IV-B, as *horizontal displacement*. This scheme is a generalization of [34] to delay-systems in form of MoC macromodels. It is aimed at collapsing the passivity violation intervals by iteratively perturbing their edges ω_k to new locations $\tilde{\omega}_k$ until passivity is obtained. Horizontal arrows in Fig. 3 provide a graphical illustration. The second scheme, developed in Section IV-D, is denoted as *vertical displacement*. This scheme is similar to the approaches in [29]–[33], since it formulates the passivity constraints at selected frequencies, by directly perturbing the eigenvalues of $\boldsymbol{G}_{1,2}$. The vertical arrows of Fig. 3 give a snapshot of this process.

The presentation of the two algorithms is organized as follows. We first recall, in Section IV-A, some general perturbation results applied to the FDEP (11), which provide the background material for the horizontal displacement scheme. The horizontal displacement scheme is then introduced in Section IV-B, followed by a list of possible strategies for accuracy preservation during the passivity enforcement, discussed in Section IV-C. The vertical displacement scheme is presented in Section IV-D. Finally, some more practical considerations on convergence and computational complexity of both schemes are provided in Section IV-E.

A. Perturbation of Frequency-Dependent Eigenvalues

This section recalls some results from [47] and [48] on first-order perturbation of the FDEP in (11). We assume that the system matrix depends on an external parameter $\varepsilon \simeq 0$. As a consequence, the eigensolution becomes parameter-dependent

$$\begin{aligned} \boldsymbol{H}(s,\varepsilon)\boldsymbol{\xi}(\varepsilon) &= s(\varepsilon)\boldsymbol{\xi}(\varepsilon) \\ \boldsymbol{\zeta}^H(\varepsilon)\boldsymbol{H}(s,\varepsilon) &= s(\varepsilon)\boldsymbol{\zeta}^H(\varepsilon) \end{aligned} \tag{24}$$

where $\boldsymbol{\xi}(\varepsilon)$ and $\boldsymbol{\zeta}(\varepsilon)$ are the right and left eigenvectors associated to the eigenvalue $s(\varepsilon)$. Neglecting higher order terms, we have the following perturbation result:

$$s(\varepsilon) \simeq s_0 + s_0'\varepsilon \tag{25}$$

where

$$s_0' = \frac{\boldsymbol{\zeta}_0^H \boldsymbol{H}_0^{(\varepsilon)} \boldsymbol{\xi}_0}{\boldsymbol{\zeta}_0^H \left(\boldsymbol{I} - \boldsymbol{H}_0^{(s)}\right) \boldsymbol{\xi}_0}. \tag{26}$$

In (26), superscript $^{(\nu)}$ denotes partial differentiation with respect to ν, and subscript $_0$ denotes evaluation for $\varepsilon = 0$. Details can be found in [52], [47], and [48]. This result will be applied in Section IV-B as an inverse perturbation scheme, in order to determine the model perturbation (here represented by the scalar variable ε) required to displace the frequency-dependent eigenvalues by a desired amount.

B. Horizontal Displacement

The horizontal displacement scheme applies the above first-order perturbation results to find new model coefficients such that the resulting MoC equations satisfy the passivity constraints (8). The particular choice of candidate coefficients for perturbation is somewhat arbitrary. In principle, all state-space matrices of $\tilde{\boldsymbol{Y}}_c(s)$ and $\tilde{\boldsymbol{P}}(s)$ in (4) can be perturbed. However, a common strategy [25]–[37] is to preserve the poles and the direct couplings, and to perturb only the residues of the rational approximations, which are usually directly stored in $\bar{\boldsymbol{C}}$ and $\hat{\boldsymbol{C}}$ for characteristic admittance and the propagation operator, respectively. In order to simplify the presentation, we consider only the perturbation of the characteristic admittance system, although the same procedure can be applied to the propagation operator. Therefore, our "free variables" will be the entries of a matrix $\bar{\boldsymbol{\Delta}}$, defined as

$$\bar{\boldsymbol{C}}_p - \bar{\boldsymbol{C}} = \bar{\boldsymbol{\Delta}} \tag{27}$$

where $\bar{\boldsymbol{C}}_p$ is the state space matrix of the perturbed system.

The derivation of all perturbation results is here detailed only for $\boldsymbol{H}_1$ of (11), similar results holding for $\boldsymbol{H}_2$. Given this assumption, we will drop the subscript $_1$ to simplify the notation.

A direct application of the results of Section IV-A for the perturbation of the kth imaginary eigenvalue leads to

$$\begin{aligned}\tilde{s}_k - s_k &= j\tilde{\omega}_k - j\omega_k \\ &\simeq \frac{\boldsymbol{\zeta}_k^H \mathrm{d}\boldsymbol{H}_k \boldsymbol{\xi}_k}{\boldsymbol{\zeta}_k^H \left(\boldsymbol{U} - \boldsymbol{H}_k^{(s)}\right)\boldsymbol{\xi}_k}\end{aligned} \tag{28}$$

where

$$\begin{aligned}\mathrm{d}\boldsymbol{H}_k &= \mathrm{d}\boldsymbol{\mathcal{V}} + \sum_{n=1}^{m}\left(\mathrm{d}\boldsymbol{\mathcal{W}}_n^- e^{-j\omega_k T_n} + \mathrm{d}\boldsymbol{\mathcal{W}}_n^+ e^{j\omega_k T_n}\right) \\ \boldsymbol{H}_k^{(s)} &= \sum_{n=1}^{m}\left(-T_n \boldsymbol{\mathcal{W}}_n^- e^{-j\omega_k T_n} + T_n \boldsymbol{\mathcal{W}}_n^+ e^{j\omega_k T_n}\right) \\ &\quad + \sum_{n=1}^{m}\sum_{l=1}^{m}(T_n - T_l)\boldsymbol{\mathcal{W}}_{n,l} e^{j\omega_k (T_n - T_l)}\end{aligned} \tag{29}$$

and

$$\begin{aligned}\mathrm{d}\boldsymbol{\mathcal{V}} &= \begin{bmatrix}\mathrm{d}\boldsymbol{\mathcal{V}}_{11} & \boldsymbol{0} \\ \mathrm{d}\boldsymbol{\mathcal{V}}_{21} & -\mathrm{d}\boldsymbol{\mathcal{V}}_{11}^T\end{bmatrix} \\ \mathrm{d}\boldsymbol{\mathcal{W}}_n^- &= \begin{bmatrix}\boldsymbol{0} & \boldsymbol{0} \\ \mathrm{d}\boldsymbol{\mathcal{W}}_{21,n}^- & \boldsymbol{0}\end{bmatrix} \\ \mathrm{d}\boldsymbol{\mathcal{W}}_n^+ &= \begin{bmatrix}\boldsymbol{0} & \boldsymbol{0} \\ (\mathrm{d}\boldsymbol{\mathcal{W}}_{21,n}^-)^T & \boldsymbol{0}\end{bmatrix}\end{aligned} \tag{30}$$

$$\begin{aligned}\mathrm{d}\boldsymbol{\mathcal{V}}_{11} &= \begin{bmatrix}\boldsymbol{0} & \boldsymbol{0} & \hat{\boldsymbol{B}}_1 \boldsymbol{\mathcal{R}}\boldsymbol{D}\bar{\boldsymbol{\Delta}} \\ \boldsymbol{0} & \boldsymbol{0} & (\hat{\boldsymbol{B}}_2 \boldsymbol{\mathcal{R}}\boldsymbol{D} + \boldsymbol{B})\bar{\boldsymbol{\Delta}} \\ \boldsymbol{0} & \boldsymbol{0} & \hat{\boldsymbol{B}}_3 \boldsymbol{\mathcal{R}}\boldsymbol{D}\bar{\boldsymbol{\Delta}}\end{bmatrix} \\ \mathrm{d}\boldsymbol{\mathcal{V}}_{21} &= \begin{bmatrix}\boldsymbol{0} & \boldsymbol{0} & \boldsymbol{0} \\ \boldsymbol{0} & \boldsymbol{0} & \boldsymbol{0} \\ \boldsymbol{0} & \boldsymbol{0} & -\bar{\boldsymbol{\Delta}}^T \boldsymbol{D}^T \boldsymbol{\mathcal{R}}\boldsymbol{D}\bar{\boldsymbol{C}} - \bar{\boldsymbol{C}}^T \boldsymbol{D}^T \boldsymbol{\mathcal{R}}\boldsymbol{D}\bar{\boldsymbol{\Delta}}\end{bmatrix}\end{aligned} \tag{31}$$

$$\mathrm{d}\boldsymbol{\mathcal{W}}_{21,n}^- = \begin{bmatrix}\boldsymbol{0} & \boldsymbol{0} & \boldsymbol{0} \\ \boldsymbol{0} & \boldsymbol{0} & \boldsymbol{0} \\ -\bar{\boldsymbol{\Delta}}^T \boldsymbol{D}^T \boldsymbol{\mathcal{R}}\boldsymbol{C}^n & \bar{\boldsymbol{\Delta}}^T \boldsymbol{D}^T \boldsymbol{\mathcal{R}}\boldsymbol{C}^n & \boldsymbol{0}\end{bmatrix}. \tag{32}$$

Since $\boldsymbol{H}(s)$ is a Hamiltonian matrix for $s = j\omega$, the left and right eigenvectors are related by $\boldsymbol{\zeta}_k = -\boldsymbol{J}\boldsymbol{\xi}_k$. Therefore, (28) becomes

$$j\tilde{\omega}_k - j\omega_k \simeq \frac{\boldsymbol{\xi}_k^H \boldsymbol{J}\mathrm{d}\boldsymbol{H}_k \boldsymbol{\xi}_k}{\boldsymbol{\xi}_k^H \boldsymbol{J}\left(\boldsymbol{U} - \boldsymbol{H}_k^{(s)}\right)\boldsymbol{\xi}_k}. \tag{33}$$

In order to derive a linear constraint between $\bar{\boldsymbol{\Delta}}$ and $\tilde{\omega}_k$, we exploit the 6×6 block structure of matrix $\mathrm{d}\boldsymbol{H}_k$, as derived in (13)–(17). Inducing the same partitioning on the eigenvector $\boldsymbol{\xi}_k = [\boldsymbol{\xi}_{k,1}^T \ldots \boldsymbol{\xi}_{k,6}^T]^T$, after some straightforward manipulations we obtain

$$\boldsymbol{\xi}_k^H \boldsymbol{J}\mathrm{d}\boldsymbol{H}_k \boldsymbol{\xi}_k = 2\Re\left\{\boldsymbol{z}_k^H \bar{\boldsymbol{\Delta}}\boldsymbol{\xi}_{k,3}\right\} \tag{34}$$

with

$$\begin{aligned}\boldsymbol{z}_k = &-\sum_{n=1}^{m}(\boldsymbol{D}^T \boldsymbol{\mathcal{R}}\boldsymbol{C}^n \boldsymbol{\xi}_{k,1} e^{-j\omega_k T_n} \\ &- \boldsymbol{D}^T \boldsymbol{\mathcal{R}}\boldsymbol{C}^n \boldsymbol{\xi}_{k,2} e^{-j\omega_k T_n}) \\ &+ \boldsymbol{D}^T \boldsymbol{\mathcal{R}}\boldsymbol{D}\bar{\boldsymbol{C}}\boldsymbol{\xi}_{k,3} + \boldsymbol{D}^T \boldsymbol{\mathcal{R}}\hat{\boldsymbol{B}}_1^T \boldsymbol{\xi}_{k,4} \\ &+ \left(\boldsymbol{D}^T \boldsymbol{\mathcal{R}}\hat{\boldsymbol{B}}_2^T + \boldsymbol{B}^T\right)\boldsymbol{\xi}_{k,5} + \boldsymbol{D}^T \boldsymbol{\mathcal{R}}\hat{\boldsymbol{B}}_3^T \boldsymbol{\xi}_{k,6}.\end{aligned} \tag{35}$$

Combining now (33) and (34), we obtain

$$\frac{2\Re\left\{\boldsymbol{\xi}_{k,3}^T \otimes \boldsymbol{z}_k^H\right\}}{\Im\left\{\boldsymbol{\xi}_k^H \boldsymbol{J}\left(\boldsymbol{U} - \boldsymbol{H}_k^{(s)}\right)\boldsymbol{\xi}_k\right\}}\mathrm{vec}\left(\bar{\boldsymbol{\Delta}}\right) \simeq \omega_k - \tilde{\omega}_k \tag{36}$$

where $\otimes$ is the Kronecker product [53] and the operator $\mathrm{vec}\left(\cdot\right)$ stacks the columns of its matrix argument. Collecting (36) for all imaginary eigenvalues leads to an underdetermined system, whose solution forces the displacement of all imaginary eigenvalues $j\omega_k$ to new target locations $j\tilde{\omega}_k$. Iterative application of the above procedure leads to passivity enforcement when the eigenvalues are perturbed inwards for each of the passivity violation intervals, as depicted in Fig. 3.

The presented horizontal displacement scheme extends the approach of [34], valid only for lumped macromodels, to delay-based MoC macromodels. The structure of the linear constraint (36) is indeed very similar to (60) of [34], although the derivation is more complicated in the MoC case due to a different internal structure of the macromodel.

C. Strategies for Accuracy Preservation

Let us examine (36) more closely. The number of linear constraints equals the number of imaginary eigenvalues of (11), whereas the number of unknowns is $n_y m^2$, where n_y is the number of poles used in the rational approximation of the characteristic admittance operator. In most practical applications the passivity violations are located at low frequencies, since conductor and dielectric losses effectively contribute to the high frequency passive behavior of the model. This typically results in a small number of imaginary eigenvalues. As a consequence, system (36) is underdetermined. This enables the inclusion of additional constraints on its solution, which can be effectively chosen so that the extent of the model perturbation is minimized, thus preserving model accuracy.

The standard approach for accuracy preservation is to enforce a minimum-norm constraint, where the particular norm must be carefully selected depending on the application. The most commonly employed norm is equivalent to the cumulative energy of the model perturbation in $\mathcal{L}^2$ sense

$$\begin{aligned}\mathcal{E} &= \frac{1}{2\pi}\sum_{ik}\int_{-\infty}^{\infty}|\mathrm{d}\tilde{Y}_{c,ik}(j\omega)|^2 \mathrm{d}\omega \\ &= \mathrm{tr}\{\bar{\boldsymbol{\Delta}}\bar{\boldsymbol{W}}\bar{\boldsymbol{\Delta}}^T\}\end{aligned} \tag{37}$$

where $\mathrm{d}\tilde{Y}_{c,ik}$ represents the perturbation of the (i,k) element of the characteristic admittance operator of the model, and $\bar{\boldsymbol{W}}$ is the associated controllability Gramian, defined as the unique symmetric and positive definite solution of the Lyapunov equation

$$\bar{\boldsymbol{A}}\bar{\boldsymbol{W}} + \bar{\boldsymbol{W}}\bar{\boldsymbol{A}}^T = -\bar{\boldsymbol{B}}\bar{\boldsymbol{B}}^T. \tag{38}$$

Consequently, the natural accuracy constraint to be associated to (36) reads

$$\min \mathrm{tr}\{\bar{\boldsymbol{\Delta}}\bar{\boldsymbol{W}}\bar{\boldsymbol{\Delta}}^T\}. \tag{39}$$

Recent developments have shown that alternative norms can be used instead of (37), leading to some advantages for specific applications. In particular, we can cite norms equivalent to the relative error [38], [39], obtained via inverse magnitude

weighting, and bandlimited norms allowing to fine-tune the accuracy metric in specific frequency bands [40]. All these cases lead to an alternative definition of the Gramian matrix $\bar{\boldsymbol{W}}$ and are therefore compatible with (39). In this work, we use both the standard $\mathcal{L}^2$ norm (37) and the relative norm [38], [39].

D. Vertical Displacement

In this section, we present an alternative perturbation scheme for MoC passivity enforcement. As outlined in Section IV and depicted in Fig. 3, the vertical displacement scheme works on the negative eigenvalues of $\boldsymbol{G}_{1,2}(s)$ defined in (8) and lifts them above the zero-level. As in Section IV-B, we consider $\boldsymbol{G}_1(s)$ only in the presentation, and we omit the subscript in order to simplify the notation. Also, the presentation of the perturbation scheme is limited to the characteristic admittance only, although the procedure is general and can be applied to the propagation operator with minor modifications.

We start by considering the results of the passivity characterization process of Section III, which outputs a set of frequency bands, delimited by the imaginary eigenvalues of (11), where passivity violations are localized. Within each of these frequency intervals Ω_k, we denote the minimum (negative) eigenvalue as λ_{J_k}, and with $\breve{\omega}_k$ the frequency where the lowest value is reached; see also Fig. 3. The direct application of a standard eigenvalue perturbation analysis [52] to the Hermitian matrix $\boldsymbol{G}$ results in

$$\tilde{\lambda}_{J_k} - \lambda_{J_k} \simeq \frac{\boldsymbol{x}_{J_k}^H \mathrm{d}\boldsymbol{G}\boldsymbol{x}_{J_k}}{\boldsymbol{x}_{J_k}^H \boldsymbol{x}_{J_k}} \tag{40}$$

where $\boldsymbol{x}_{J_k}$ is the right (left) eigenvector of $\boldsymbol{G}$ corresponding to the eigenvalue λ_{J_k} and where $\mathrm{d}\boldsymbol{G}$ is the matrix perturbation required for a first-order relocation of λ_{J_k} into $\tilde{\lambda}_{J_k}$. This perturbation is now expressed in terms of the characteristic admittance perturbation $\bar{\boldsymbol{\Delta}}$. Using (8) and (9), we obtain

$$\boldsymbol{x}_{J_k}^H \mathrm{d}\boldsymbol{G}\boldsymbol{x}_{J_k} = 2\Re\left\{\bar{\boldsymbol{y}}_k^H \bar{\boldsymbol{\Delta}} \bar{\boldsymbol{z}}_k\right\} \tag{41}$$

where

$$\begin{aligned} \bar{\boldsymbol{y}}_k^H &= \boldsymbol{x}_{J_k}^H \boldsymbol{W}_+^{-1}(j\breve{\omega}_k)\boldsymbol{W}_-(j\breve{\omega}_k) \\ \bar{\boldsymbol{z}}_k &= (j\breve{\omega}_k \boldsymbol{U} - \bar{\boldsymbol{A}})^{-1}\bar{\boldsymbol{B}}\boldsymbol{x}_{J_k}. \end{aligned} \tag{42}$$

Using now the properties of the Kronecker product and assuming that $\|\boldsymbol{x}_{J_k}\| = 1$, we obtain

$$\boldsymbol{x}_{J_k}^H \mathrm{d}\boldsymbol{G}\boldsymbol{x}_{J_k} = 2\Re\left\{\bar{\boldsymbol{z}}_k^T \otimes \bar{\boldsymbol{y}}_k^H\right\} \mathrm{vec}\,(\bar{\boldsymbol{\Delta}}). \tag{43}$$

Combining now the passivity constraint $\tilde{\lambda}_{J_k} \geq 0$ with (40) and (43), we have the final result

$$2\Re\left\{\bar{\boldsymbol{z}}_k^T \otimes \bar{\boldsymbol{y}}_k^H\right\} \mathrm{vec}\,(\bar{\boldsymbol{\Delta}}) \geq -\lambda_{J_k}. \tag{44}$$

A set of linear inequality constraints is obtained by writing (44) for all passivity violation intervals. Combined with the minimum norm condition (39), this set of inequalities results in a linearly-constrained quadratic optimization program, which can be efficiently solved using standard convex optimization techniques [56]. We remark that the above vertical displacement scheme is a direct extension of the results in [29], [30], [32], [33], which hold for lumped (delayless) macromodels only.

E. Computational Complexity and Practical Considerations

In this section, we compare the computational complexity of horizontal and vertical displacement schemes, by providing the relevant operations count scaling with the number of ports/poles of the macromodel.

Each step of the horizontal displacement algorithm requires the solution of an underdetermined system with K_1 equations and $m^2 \times n_y$ free variables, where K_1 is the number of imaginary eigenvalues of FD-EP, m is the number of coupled lines and n_y is the number of poles used in the rational approximation of $\boldsymbol{Y}_c$. As explained in [54] the required computational complexity is $O(K_1 m^4 n_y^2)$. Instead, each step of the vertical displacement method involves a linearly constrained quadratic optimization problem with K_2 constraints and $m^2 \times n_y$ free variables again, where K_2 is the number of nonpassive frequency bands ($K_2 < K_1$). The computational complexity of this type of problems cannot be provided explicitly, since iterative schemes are used, with results that depend on the particular implementation. However, it can be proved that such quadratic optimization problems have at most polynomial computational complexity. A pessimistic estimate given in [55] reads $O((K_2 + m^2 n_y)^4)$, which is consistent with the discussion in [25].

An upper bound for the number of iterations is very difficult to find, even on a statistical basis. In general, the experimental results of all tested examples show that the number of iterations required by the horizontal and vertical displacement schemes is very similar. The actual figures for each example are reported in Section V.

A final remark on convergence. Both discussed methods are based on perturbation. In principle, there is no guarantee that the model perturbation based on a local constraint in a given passivity violation region will not create other passivity violations at different frequency points, especially out of the frequency range of interest. However, the specific accuracy constraints discussed in Section IV-C guarantee a minimal model perturbation throughout the frequency axis. Therefore, in case a new passivity violation arises, it is guaranteed to be very small, hence easy to be removed at the next iteration. In addition, new out-of-band passivity violations are not a practical issue for the structures that we are interested here, since high-frequency losses (both metal and dielectric) do guarantee significant energy attenuation outside the modeling bandwidth. In fact, the passivity violations for all investigated test cases are actually concentrated in the low frequency range, where the interconnect is nearly lossless. As a result, local constraints prove to be sufficient for global passivity enforcement.

V. Examples

A. Microstrip Line

The first example we consider is a single $\mathcal{L} = 10$ cm microstrip line, whose cross-sectional geometry is specified in Fig. 4. The frequency-dependent per-unit-length parameters have been computed over a broad frequency range, from dc up to 10 GHz, using a combination of the 2-D method-of moments (MoM) techniques of [50] and [51]. Then, an initial MoC macromodel in the form (2)–(4) has been derived using the standard delay extraction process combined with vector

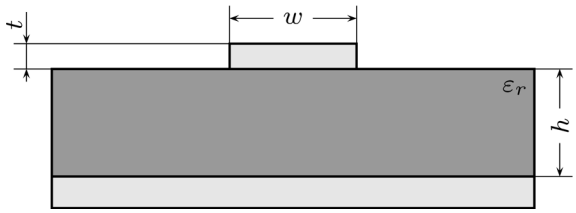

Fig. 4. Geometry specification for the microstrip example of Section V-A. Parameter values are $\varepsilon_r = 4.7, t = 1.4$ mils, $h = 1/16''$, $w = 7$ mils.

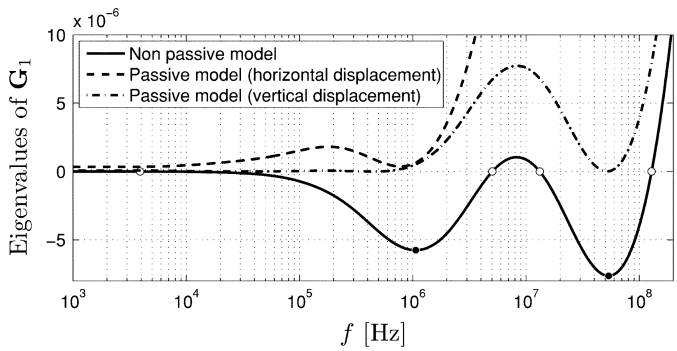

Fig. 5. Passivity enforcement of the microstrip example of Section V-A. The first eigenvalue is depicted before (solid line) and after passivity enforcement using horizontal (dashed line) and vertical (dash-dot line) displacement schemes.

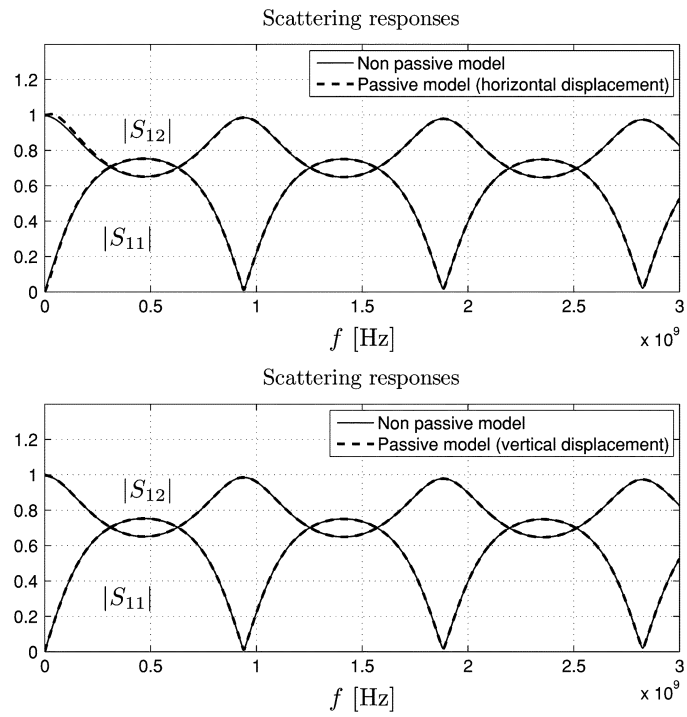

Fig. 6. Scattering frequency responses of the microstrip line macromodel before and after passivity enforcement via horizontal (top) and vertical (bottom) displacement. The scattering responses obtained via direct frequency-domain solution of (1) are not reported since undistinguishable from those of the nonpassive macromodel.

fitting (VF). Six poles were used in the rational approximation (4) of both characteristic admittance and propagation operator. Application of the passivity check outlined in Section III highlights two frequency bands where the eigenvalue of $\boldsymbol{G}_1$ (a scalar quantity in this case) is negative, as depicted in Fig. 5, with four purely imaginary eigenvalues of the FDEP (11). All eigenvalues of $\boldsymbol{G}_2$ are instead uniformly positive.

Application of the proposed horizontal displacement scheme leads to passivity compensation in only one iteration, with a total runtime of about 0.4 s on a notebook (1.66 GHz CPU). Conversely, the vertical displacement scheme generates a passive model in three iterations, with a total runtime of 0.44 s on the same hardware. The results are depicted in Fig. 6, where the scattering responses of all models are compared. These plots show that the accuracy is well-preserved during passivity compensation. The maximum deviation (computed among all responses and all frequency samples) from the raw scattering responses obtained via direct frequency-domain solution of (1) was 0.0025, 0.0027, and 0.0345 for nonpassive, vertical-displacement based and horizontal-displacement based passive models, respectively. We remark that the vertical displacement scheme provides slightly better accuracy with respect to the horizontal scheme, as can be noted also from Fig. 5. This fact will be further confirmed also for the other test cases analyzed in this work.

Fig. 7 reports the transient port responses of nonpassive and passive macromodels to a trapezoidal voltage pulse applied on one end of the line with 50 Ω terminations. Both passive macromodels produce very consistent results. However, changing the termination into a simple RL load drives the nonpassive model to instability, while the passive models remains well-behaved; see Fig. 8. This plot is a further confirmation that passivity is

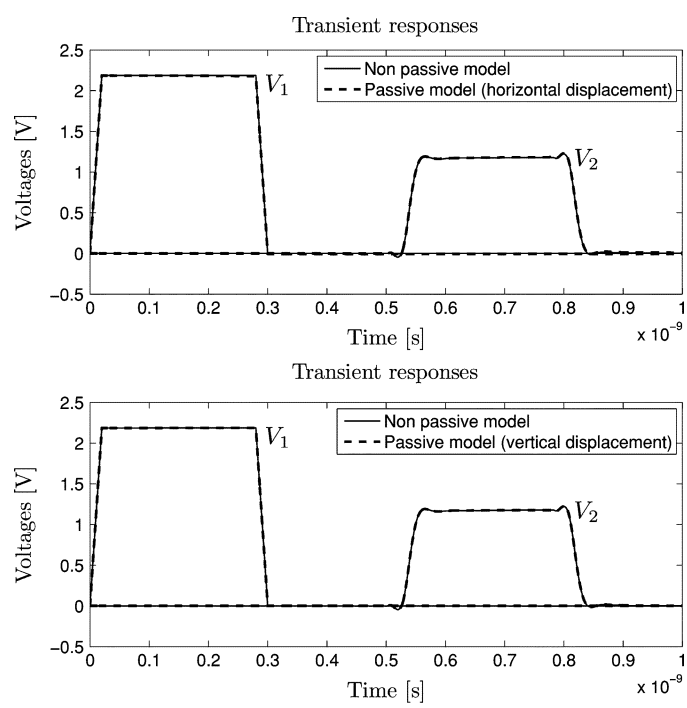

Fig. 7. Transient responses (obtained with SPICE) of the microstrip line macromodel before and after passivity enforcement via horizontal (top) and vertical (bottom) displacement.

a fundamental property that must be guaranteed in any macromodel. In both cases, a SPICE realization of the macromodel with standard circuit elements was used. The required CPU time

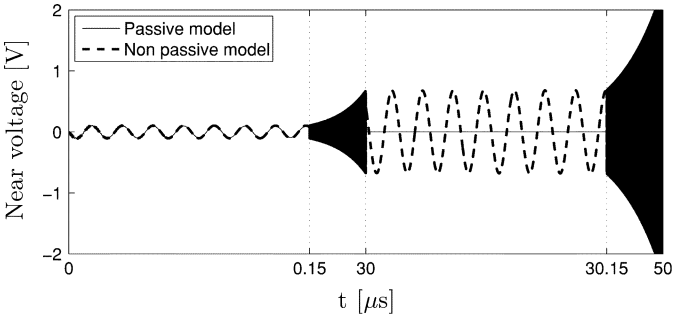

Fig. 8. Nonpassive microstrip line macromodel looses stability when loaded by a simple $R_1 \| (R_2 + sL)$ termination at all ports (component values $R_1 = 281\,\mathrm{k}\Omega$, $R_2 = 8.90\,\mathrm{m}\Omega$, $L = 4.61\,\mu\mathrm{H}$. A nonuniform (piecewise linear) scale for the time axis is used to highlight the instability.

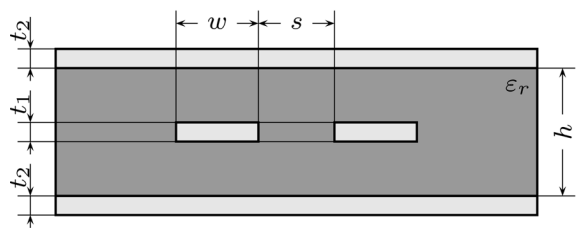

Fig. 9. Geometry specification for the coupled stripline example of Section V-B. Parameter values are $\varepsilon_r = 4.7, t_1 = 40\,\mu\mathrm{m}$, $t_2 = 17.5\,\mu\mathrm{m}$, $h = 20$ mils, $w = 6$ mils, and $s = 6$ mils.

was 0.65 s and 108 s for the results of Fig. 7 and Fig. 8, respectively. It should be noted that a kernel-based implementation of the macromodel [24] would achieve the same results with a much reduced runtime.

B. Two-Conductor Coupled Stripline

The second example is a 3-cm two-conductor coupled stripline having a cross section depicted in Fig. 9. The same procedure described in Section V-A was applied to derive a MoC macromodel, which resulted nonpassive. Fig. 10 depicts the three distinct passivity violation intervals and the 12 imaginary eigenvalues of the FDEP (11) for $\boldsymbol{G}_1$ (subsystem $\boldsymbol{G}_2$ does not show any passivity violation). Application of horizontal displacement scheme leads to passivity enforcement in three iterations, with a total runtime of 5.0 s. Vertical displacement scheme required five iterations in 5.9 s. The eigenvalue perturbation results for both schemes are reported in Fig. 10, which shows that the performance of the vertical displacement scheme is notably better than the horizontal scheme. Fig. 11 depicts one of the scattering responses of passive and nonpassive macromodels. The maximum deviation (computed among all responses and all frequency samples) from the raw scattering responses obtained via direct frequency-domain solution of (1) was 0.0010, 0.0032, and 0.0048 for nonpassive, vertical-displacement based and horizontal-displacement based passive models, respectively.

C. Five-Conductor Coupled Stripline

The last example is more challenging. A 10-cm five-conductor stripline structure is depicted in Fig. 12. A MoC macromodel was derived as for previous examples, and the proposed

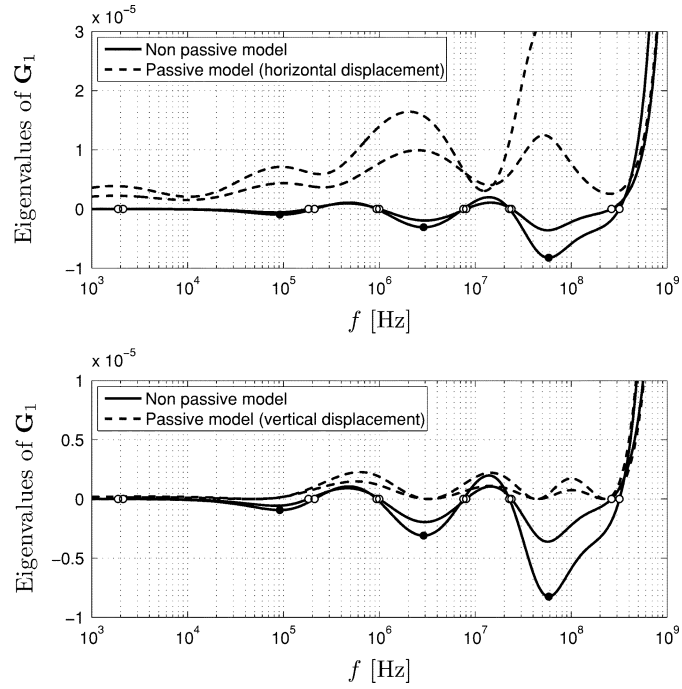

Fig. 10. Passivity enforcement of the coupled stripline of Section V-B. Top and bottom panels report the results of the horizontal and vertical displacement schemes, respectively.

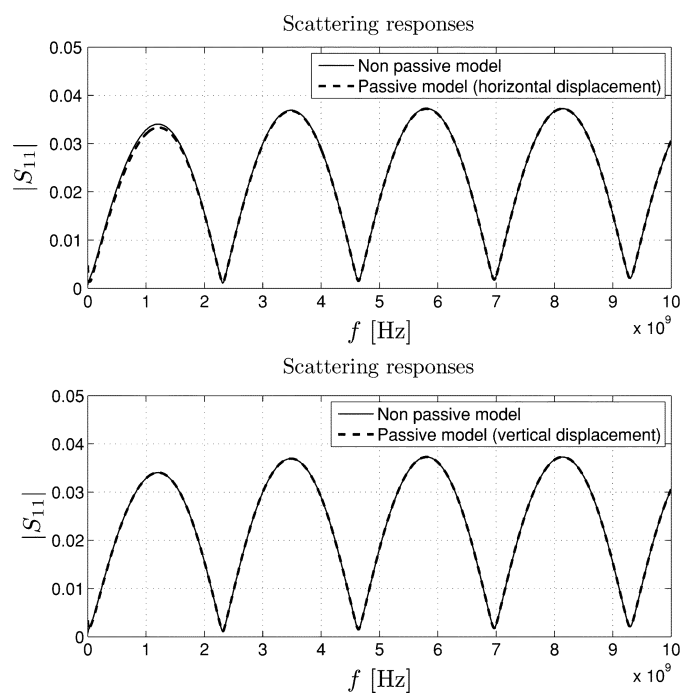

Fig. 11. Scattering response (S_{11}) of nonpassive and passive macromodels of the 2-conductor stripline of Section V-B. The scattering responses obtained via direct frequency-domain solution of (1) are not reported since undistinguishable from those of the nonpassive macromodel. Similar results were observed for other scattering responses.

passivity checking procedure was applied. The results are depicted in Fig. 2. Four passivity violation intervals are detected using the adaptive sampling process described in Section III. As a byproduct, a total of 44 eigenvalue intersections with the zero-level are found, which correspond to the imaginary eigenvalues

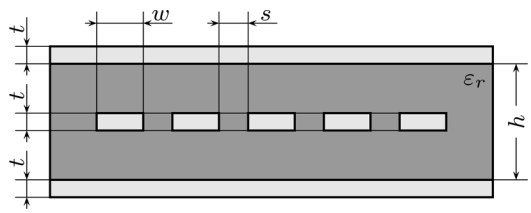

Fig. 12. Geometry specification for the coupled stripline example of Section V-C. Parameter values are $\varepsilon_r = 4.7, t = 10\,\mu$m, $h = 100\,\mu$m, $w = 20\,\mu$m, and $s = 10\,\mu$m.

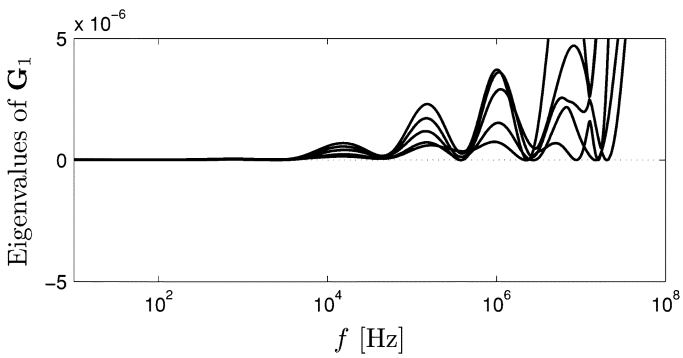

Fig. 13. Passivity enforcement of the 5-conductor stripline of Section V-C via vertical displacement. The passivity violation intervals depicted in Fig. 2 have been removed completely.

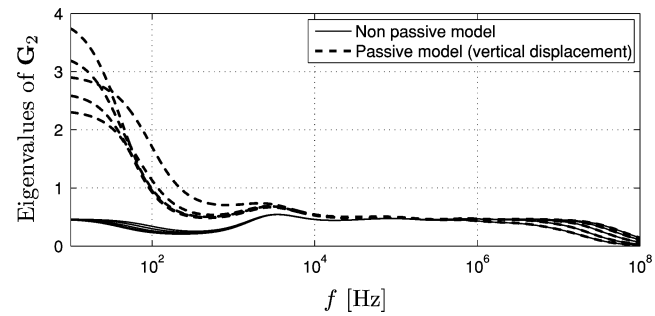

Fig. 14. Comparison of $\boldsymbol{G}_2$ eigenvalues for nonpassive and passive macromodels of the 5-conductor stripline of Section V-C.

of (11). Unfortunately, the direct solution of (11) failed, due to the presence of several clustered eigenvalues, which leads to numerical ill-conditioning. Due to these difficulties, the eigenvalues can only be computed with insufficient precision to ascertain if they are purely imaginary or not. Several linear algebra packages were tested, including HAPACK [57] and the polynomial eigenvalue routines available in MATLAB [56], leading to the same negative results.

The above ill-conditioning severely affects also the horizontal displacement scheme, which failed to converge. Conversely, no problems were encountered by the vertical displacement scheme, which computed a passive macromodel in ten iterations and 124 s. We remark that 121 s were spent by the adaptive sampling process for the passivity check, and only 3 s were required for the solution of (44). The results of the passivity enforcement are depicted in Fig. 13, showing that all violation intervals have been removed and all eigenvalues of $\boldsymbol{G}_1$ are positive at all frequencies.

VI. Discussion and Future Directions

This paper contributed several results towards the generation of guaranteed passive macromodels for transmission line structures. Assuming a model structure derived from the generalized method of characteristics (MoC), Section III discussed two alternative methods for checking the model passivity. The first method is based on the direct solution of a frequency-dependent eigenvalue problem (FDEP), first derived in [45], whereas the second method is based on an iterative sampling and tracking process. The presented numerical examples show that the latter seems to be more reliable and robust when the number of line conductors increases. This is mainly due to the numerical difficulties arising in the solution of the nonlinear eigenvalue problem (11).

The main contributions of this work are two alternative methods for enforcing the passivity of a MoC-based macromodel. The first method, named horizontal displacement scheme, performs an iterative perturbation of purely imaginary eigenvalues of a FDEP, thus extending the technique of [34] to the case of delayed macromodels. The second method, named vertical displacement scheme, solves a linearly constrained quadratic optimization aimed at enforcing the positive realness of the macromodel admittance matrix at carefully selected frequency points. It turns out that the latter is more reliable and robust, again due to the intrinsic numerical difficulties in handling the aforementioned FDEP. The general conclusion is that the combination of adaptive sampling and constrained optimization provides an accurate and efficient way of correcting and removing passivity violations in MoC-based transmission line macromodels.

Some open problems remain and are now discussed. Despite the explicit accuracy preservation constraints that are used during passivity enforcement (see Section IV-C), the perturbation induced in the model responses may be too large for practical applications. As a demonstration, we consider again the five-conductor stripline example of Section V-C. Fig. 13 shows the passivity-enforced eigenvalues of $\boldsymbol{G}_1$. In Fig. 14, we report instead the eigenvalues of $\boldsymbol{G}_2$, computed using the passive macromodel obtained from the vertical displacement scheme. We remark that these eigenvalues were uniformly positive in the original nonpassive macromodel (also shown in the plot), so that no direct perturbation was applied to them during passivity enforcement. Fig. 14 shows that these eigenvalues undergo a quite significant perturbation in the low frequencies range. This can be readily explained from the structure of (8) and (9). It can be noted that $\boldsymbol{G}_2$ assumes large values (hence large eigenvalues) at low frequencies, due to numerical cancellation effects in the matrix to be inverted. This causes large sensitivities of the $\boldsymbol{G}_2$ entries to any model perturbation. This fact is intrinsic in the MoC model structure and independent on the perturbation approach being devised for passivity enforcement. As a further confirmation, Fig. 15 compares selected scattering responses of nonpassive and passive models. Although some responses remain well-behaved and accurate, some other responses are excessively deteriorated at low frequencies.

Various countermeasures were attempted in order to preserve a good low-frequency macromodel behavior, including relative

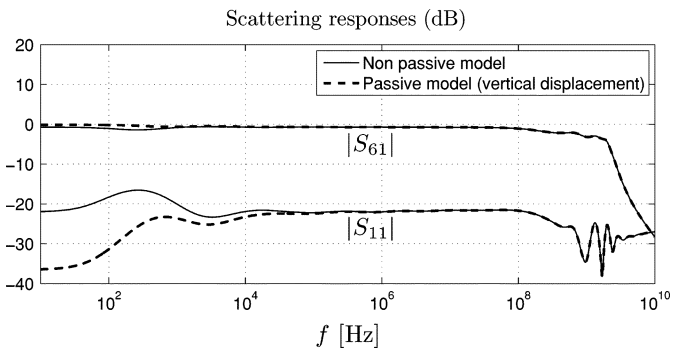

Fig. 15. Selected scattering responses of nonpassive and passive macromodels of the 5-conductor stripline of Section V-C.

error control [38], [39] and hard constraints on the dc macromodel response added to (44). Both approaches did not provide significantly different results. Therefore, although the presented techniques seem to provide efficient and sufficiently accurate results for passivity enforcement of low-complexity transmission line macromodels, further work is needed for a robust solution of general applicability.

REFERENCES

[1] B. Gustavsen and A. Semlyen, "Rational approximation of frequency domain responses by vector fitting," *IEEE Trans. Power Del.*, vol. 14, no. 3, pp. 1052–1061, Jul. 1999.

[2] B. Gustavsen, "Computer code for rational approximation of frequency dependent admittance matrices," *IEEE Trans. Power Del.*, vol. 17, no. 4, pp. 1093–1098, Oct. 2002.

[3] B. Gustavsen and A. Semlyen, "A robust approach for system identification in the frequency domain," *IEEE Trans. Power Del.*, vol. 19, no. 3, pp. 1167–1173, Jul. 2004.

[4] D. Deschrijver and T. Dhaene, "Rational modeling of spectral data using orthonormal vector fitting," in *Proc. 9th IEEE Workshop Signal Propagation Interconnects*, Garmisch-Partenkirchen, Germany, May 10–13, 2005, pp. 111–114.

[5] D. Deschrijver, B. Haegeman, and T. Dhaene, "Orthonormal vector fitting: A robust macromodeling tool for rational approximation of frequency domain responses," *IEEE Trans. Adv. Packag.*, vol. 30, no. 2, pp. 216–225, May 2007.

[6] S. Grivet-Talocia and M. Bandinu, "Improving the convergence of vector fitting in presence of noise," *IEEE Trans. Electromagn. Compat.*, vol. 48, no. 1, pp. 104–120, Feb. 2006.

[7] W. Beyene and J. Schutt-Ainé, "Accurate frequency-domain modeling and efficient circuit simulation of high-speed packaging interconnects," *IEEE Trans. Microw. Theory Tech.*, vol. 45, no. 10, pp. 1941–1947, Oct. 1997.

[8] K. L. Choi and M. Swaminathan, "Development of model libraries for embedded passives using network synthesis," *IEEE Trans. Circuits Syst. II*, vol. 47, no. 4, pp. 249–260, Apr. 2000.

[9] M. Elzinga, K. Virga, L. Zhao, and J. L. Prince, "Pole-residue formulation for transient simulation of high-frequency interconnects using householder LS curve-fitting techniques," *IEEE Trans. Comp. Packag. Manufact. Technol.*, vol. 23, no. 2, pp. 142–147, Mar. 2000.

[10] M. Elzinga, K. Virga, and J. L. Prince, "Improve global rational approximation macromodeling algorithm for networks characterized by frequency-sampled data," *IEEE Trans. Microw. Theory Tech.*, vol. 48, no. 9, pp. 1461–1467, Sep. 2000.

[11] J. Morsey and A. C. Cangellaris, "PRIME: Passive realization of interconnect models from measured data," in *Proc. IEEE 10th Topical Meeting Electr. Performance Electron. Packag.*, Cambridge, MA, 2001, pp. 47–50.

[12] IdEM 2.4 [Online]. Available: http://www.emc.polito.it

[13] M. Nakhla and R. Achar, "Simulation of high-speed interconnects," *Proc. IEEE*, vol. 89, no. 5, pp. 693–728, May 2001.

[14] M. Celik, L. Pileggi, and A. Obadasioglu, *IC Interconnect Analysis*. Norwell, MA: Kluwer, 2002.

[15] A. Dounavis, R. Achar, and M. Nakhla, "Efficient passive circuit models for distributed networks with frequency-dependent parameters," *IEEE Trans. Adv. Packag.*, vol. 23, no. 3, pp. 382–392, Aug. 2000.

[16] A. Dounavis, R. Achar, and M. Nakhla, "A general class of passive macromodels for lossy multiconductor transmission lines," *IEEE Trans. Microw. Theory Tech.*, vol. 49, no. 10, pp. 1686–1696, Oct. 2001.

[17] Q. Yu, J. M. L. Wang, and E. S. Kuh, "Passive multipoint moment matching model order reduction algorithm on multiport distributed interconnect networks," *IEEE Trans. Circuits Syst. I*, vol. 46, no. 1, pp. 140–160, Jan. 1999.

[18] N. M. Nakhla, A. Dounavis, R. Achar, and M. S. Nakhla, "DEPACT: Delay extraction-based passive compact transmission-line macromodeling algorithm," *IEEE Trans. Adv. Packag.*, vol. 28, no. 1, pp. 13–23, Feb. 2005.

[19] F. H. Branin Jr., "Transient analysis of lossless transmission lines," *Proc. IEEE*, vol. 55, no. 11, pp. 2012–2013, Nov. 1967.

[20] A. J. Gruodis and C. S. Chang, "Coupled lossy transmission line characterization and simulation," *IBM J. Res. Develop.*, vol. 25, pp. 25–41, Jan. 1981.

[21] F. Y. Chang, "The generalized method of characteristics for waveform relaxation analysis of lossy coupled transmission lines," *IEEE Trans. Microw. Theory Tech.*, vol. 37, no. 12, pp. 2028–2038, Dec. 1989.

[22] S. Lin and E. S. Kuh, "Transient simulation of lossy interconnects based on the recursive convolution formulation," *IEEE Trans. Circuits Syst. I*, vol. 39, no. 11, pp. 879–892, Nov. 1992.

[23] D. B. Kuznetsov and J. E. Schutt-Ainé, "Optimal transient simulation of transmission lines," *IEEE Trans. Circuits Syst. I*, vol. 43, no. 2, pp. 110–121, Feb. 1996.

[24] S. Grivet-Talocia, H. M. Huang, A. E. Ruehli, F. Canavero, and I. M. Elfadel, "Transient analysis of lossy transmission lines: An efficient approach based on the method of characteristics," *IEEE Trans. Adv. Packag.*, vol. 27, no. 1, pp. 45–56, Feb. 2004.

[25] C. P. Coelho, J. Phillips, and L. M. Silveira, "A convex programming approach for generating guaranteed passive approximations to tabulated frequency-data," *IEEE Trans. Comput.-Aided Design Integr. Circuits Syst.*, vol. 23, no. 2, pp. 293–301, Feb. 2004.

[26] H. Chen and J. Fang, "Enforcing bounded realness of S parameter through trace parameterization," in *Proc. Electr. Performance Electron. Packag.*, Princeton, NJ, Oct. 27–29, 2003, pp. 291–294.

[27] B. Dumitrescu, "Parameterization of positive-real transfer functions with fixed poles," *IEEE Trans. Circuits Syst. I*, vol. 49, no. 4, pp. 523–526, Apr. 2002.

[28] S. Grivet-Talocia, "Enforcing passivity of macromodels via spectral perturbation of hamiltonian matrices," in *Proc. 7th IEEE Workshop Signal Propagation Interconnects*, Siena, Italy, May 11–14, 2003, pp. 33–36.

[29] B. Gustavsen and A. Semlyen, "Enforcing passivity for admittance matrices approximated by rational functions," *IEEE Trans. Power Syst.*, vol. 16, no. 1, pp. 97–104, Feb. 2001.

[30] B. Gustavsen, "Computed code for passivity enforcement of rational macromodels by residue perturbation," *IEEE Trans. Adv. Packag.*, vol. 30, no. 2, pp. 209–215, May 2007.

[31] D. Saraswat, R. Achar, and M. Nakhla, "Enforcing passivity for rational function based macromodels of tabulated data," in *Proc. Electr. Performance Electron. Packag.*, Princeton, NJ, Oct. 27–29, 2003, pp. 295–298.

[32] D. Saraswat, R. Achar, and M. Nakhla, "A fast algorithm and practical considerations for passive macromodeling of measured/simulated data," *IEEE Trans. Comp., Packag. Manuf. Technol.*, vol. 27, no. 1, pp. 57–70, Feb. 2004.

[33] D. Saraswat, R. Achar, and M. Nakhla, "Global passivity enforcement algorithm for macromodels of interconnect subnetworks characterized by tabulated data," *IEEE Trans. Very Large Scale Integr. Syst.*, vol. 13, no. 7, pp. 819–832, Jul. 2005.

[34] S. Grivet-Talocia, "Passivity enforcement via perturbation of hamiltonian matrices," *IEEE Trans. Circuits Syst. I*, vol. 51, no. 9, pp. 1755–1769, Sep. 2004.

[35] S. Grivet-Talocia and A. Ubolli, "On the generation of large passive macromodels for complex interconnect structures," *IEEE Trans. Adv. Packag.*, vol. 29, no. 1, pp. 39–54, Feb. 2006.

[36] S. Grivet-Talocia, "Improving the efficiency of passivity compensation schemes via adaptive sampling," in *Proc. 14th IEEE Topical Meeting Electr. Performance Electron. Packag.*, Austin, TX, Oct. 24–26, 2005, pp. 231–234.

[37] S. Grivet-Talocia, "An adaptive sampling technique for passivity characterization and enforcement of large interconnect macromodels," *IEEE Trans. Adv. Packag.*, vol. 30, no. 2, pp. 226–237, May 2007.
[38] S. Grivet-Talocia and A. Ubolli, "On relative error minimization in passivity enforcement schemes," in *Proc. 11th IEEE Workshop Signal Propagation Interconnects*, Genova, Italy, May 13–16, 2007, pp. 75–78.
[39] S. Grivet-Talocia and A. Ubolli, "Passivity enforcement with relative error control," *IEEE Trans. Microw. Theory Tech.*, vol. 55, no. 11, pp. 2374–2383, Nov. 2007.
[40] A. Ubolli and S. Grivet-Talocia, "Weighting strategies for passivity enforcement schemes," presented at the 16th IEEE Topical Meeting Electr. Performance Electron. Packag., Atlanta, GA, Oct. 29–31, 2007.
[41] B. Gustavsen, "Fast passivity enforcement of rational macromodels by perturbation of residue matrix eigenvalues," in *11th IEEE Workshop Signal Propagation Interconnects*, Genova, Italy, May 13–16, 2007, pp. 71–74.
[42] A. Lamecki and M. Mrozowski, "Passive SPICE networks from non-passive data," presented at the 16th Int. Microw., Radar, Wireless Commun. Mikon Conf., 2006.
[43] A. Lamecki and M. Mrozowski, "Equivalent SPICE circuits with guaranteed passivity from nonpassive models," *IEEE Trans. Microw. Theory Tech.*, vol. 55, no. 3, pp. 526–532, Mar. 2007.
[44] E. Gad, C. Chen, M. Nakhla, and R. Achar, "A passivity checking algorithm for delay-based macromodels of lossy transmission lines," in *Proc. 9th IEEE Workshop Signal Propagation Interconnects*, May 10–13, 2005, pp. 125–128.
[45] E. Gad, C. Chen, M. Nakhla, and R. Achar, "Passivity verification in delay-based macromodels of electrical interconnects," *IEEE Trans. Circuits Syst. I*, vol. 52, no. 10, pp. 2173–2187, Oct. 2005.
[46] C. Chen, E. Gad, M. Nakhla, and R. Achar, "Passivity verification in delay-based macromodels of multiconductor electrical interconnects," *IEEE Trans. Adv. Packag.*, vol. 30, no. 2, pp. 246–256, May 2007.
[47] A. Chinea and S. Grivet-Talocia, "A passivity enforcement scheme for delay-based transmission line macromodels," *IEEE Microw. Wireless Compon. Lett.*, vol. 17, no. 8, pp. 562–564, Aug. 2007.
[48] A. Chinea and S. Grivet-Talocia, "Generation of passive macromodels for lossy multiconductor transmission lines," presented at the 18th Int. Zurich Symp. Electromagn. Compat., Munich, Germany, Sep. 24–28, 2007.
[49] V. A. Pothiwala and A. Dounavis, "Efficient passive transmission line macromodeling algorithm using method of characteristics," in *Proc. IEEE Int. Symp. Circuits Syst. (ISCAS)*, May 2006, pp. 1780–1783.
[50] C. Wei, R. F. Harrington, J. R. Mautz, and T. Sarkar, "Multiconductor transmission lines in multilayered delectric media," *IEEE Trans. Microw. Theor. Tech.*, vol. MTT-32, no. 4, pp. 439–450, Apr. 1984.
[51] K. M. Coperich, J. Morsey, V. I. Okhmatovski, A. C. Cangellaris, and A. E. Ruehli, "Systematic development of transmission-line models for interconnects with frequency-dependent losses," *IEEE Trans. Microw. Theory Tech.*, vol. 49, no. 10, pp. 1677–1685, Oct. 2001.
[52] J. H. Wilkinson, *The Algebraic Eigenvalue Problem*. London, U.K.: Oxford Univ. Press, 1965.
[53] J. W. Brewer, "Kronecker products and matrix calculus in system theory," *IEEE Trans. Circuits Syst.*, vol. CS-25, no. 9, pp. 772–781, Sep. 1978.
[54] G. H. Golub and C. F. Van Loan, *Matrix Computations*, 3rd ed. Baltimore, MD: Johns Hopkins Univ. Press, 1996.
[55] M. K. Kozlov, S. P. Tarasov, and L. G. Khachiyan, "Polynomial solvability of convex quadratic programming," *Dokl. Akad. Nauk SSSR*, vol. 5, pp. 1051–1053, 1979.
[56] Matlab Release 14 User's Guide [Online]. Available: http://www.mathworks.com
[57] HAPACK—Software for (Skew-)Hamiltonian Eigenvalue Problems. [Online]. Available: http://www.tu-chemnitz.de/mathematik/hapack/

Alessandro Chinea received the Laurea Specialistica (M.S.) degree in electronic engineering, in 2006, from the Politechnic University of Turin, Turin, Italy, where he is currently pursuing the Ph.D. degree.

His research interests concern macromodeling of electrical interconnects for electromagnetic compatibility and signal integrity problems. In particular, he works on algorithms development for passivity check and enforcement of distributed models.

Mr. Chinea received the Optime Award from the Unione Industriale di Torino and he was selected for the IBM EMEA Best Student Recognition Event 2006

Stefano Grivet-Talocia (M'98–SM'07) received the Laurea and Ph.D. degrees in electronic engineering from the Politechnic University of Turin, Turin, Italy.

From 1994 to 1996, he was with the NASA/Goddard Space Flight Center, Greenbelt, MD, where he worked on applications of fractal geometry and wavelet transform to the analysis and processing of geophysical time series. Currently, he is an Associate Professor of circuit theory with the Department of Electronics, Polytechnic of Turin. His current research interests are in passive macromodeling of lumped and distributed interconnect structures, modeling and simulation of fields, circuits, and their interaction, wavelets, time-frequency transforms, and their applications. He is author of more than 90 journal and conference papers.

Dr. Grivet-Talocia received the IBM Shared University Research (SUR) Award in 2007. He served as Associate Editor for the IEEE TRANSACTIONS ON ELECTROMAGNETIC COMPATIBILITY from 1999 to 2001.